Asian Journal of Chemistry; Vol. 33, No. 10 (2021), 2393-2399

ASIAN JOURNAL OF CHEMISTRY

https://doi.org/10.14233/ajchem.2021.23342

Impact of Aluminium on ZnO Thin Films for Antimicrobial Activity

BA. ANANDH[1,*], R. SAKTHIVEL[1], A. SHANKAR GANESH[1], S. SUBRAMANI[1] and A.T. RAJAMANICKAM[2]

[1]Department of Electronics, PSG College of Arts & Science, Coimbatore-641014, India
[2]Department of Electronics, Sri Ramakrishna Mission Vidyalaya College of Arts & Science, SRKV Post, Coimbatore-641020, India

*Corresponding author: E-mail: anandh.ba@gmail.com

Received: 29 May 2021; *Accepted*: 26 July 2021; *Published online*: 20 September 2021; AJC-20512

Thin films of pure zinc oxide (ZnO) and aluminium (Al) doped ZnO were deposited by two step SILAR technique. Pure and Al (1%, 3%, 5%) doped ZnO thin film's structural, morphology and optical properties were analyzed. Diffraction peaks of all the samples were indexed to hexagonal Wurtizite structure. The crystallite size, lattice parameters, dislocation density and microstrain were calculated for the prepared thin films. Morphology study using FESEM shows spherical shaped structure of pure ZnO and hexagonal faced rod like structure for Al doped ZnO thin films. The UV-vis absorption spectrum for the thin films was also studied. There is decrease in bandgap as the Al doping ratio increases from 1% to 5%. Photoluminescence studies confirmed that oxygen ion vacancy and interstitial Zn^+ ion were present. The maximum zone of inhibition was studied against the Gram-negative (*E. coli*) and Gram-positive (*S. aureus*) bacteria by agar diffusion method. Significant antimicrobial results were seen in pure and Al doped ZnO. Aluminium doped ZnO shows more antimicrobial activity over pure ZnO.

Keywords: Aluminium, Doped Zinc oxide, Hexagonal Wurtzite structure, Antimicrobial activity.

INTRODUCTION

Studies on thin films have improved several novel parts of analysis, which depends on the exclusive characteristic and structures [1]. ZnO has very good chemical stability, excellent thermal stability, high exciting binding energy (60 meV) and wide bandgap (3.37 eV) at room temperature. ZnO thin films have good electrical and optical properties, very high electrical resistivity, low cost and are non-toxic [2].

The inorganic compound ZnO has also good resistance against microorganisms [3]. ZnO is an important material for preventing the influence of food pathogens *viz*. *Staphylococcus aureus* and *Escherichia coli* on the food items [4]. It is also useful in skin treating products like ointments, diaper rashes, baby powder, *etc*. ZnO also has good antifungal activity [5], which is used for protecting the wood from fungal activity [6]. Pure ZnO films are found to unstable because of chemisorptions and adsorption that modifies the surface conductance [7]. By adding anionic and cationic dopant such as Cu, Sn, Mn, Ag, Fe, Mg and Al, the properties of zinc oxide can be modified and the thin films greatly conductive, which could be the other options for cheaper transparent conducting layers for various applications like antibacterial, antifungal, gas sensing, photocatalytic properties and solar cell [8-11], *etc*. Among the dopants, aluminum is one of the best dopant to get thin films of both transparent and conductive in the visible region. So, it can be used in transparent conductive composites. Currently, preparation of thin films has number of deposition techniques like dip coating, sputtering, chemical bath deposition, spray pyrolysis, sol-gel deposition and successive ionic layer adsorption and reaction (SILAR) [12-17]. Among these, SILAR is one of the commonly used techniques for preparing thin films because of its ease, inexpensive, non-vacuum technique and even coating over a larger area.

The aim of the present study is to prepare pure and Al doped ZnO thin films by SILAR technique and to investigate the structural, surface morphology, optical property and the biological activity of the prepared films.

EXPERIMENTAL

Glass slide was taken as substrate for depositing pure and Al doped ZnO thin films by SILAR technique. Zinc acetate dihydrates (ZAD) and aluminium acetate were used as source

and dopant material for preparing the thin films. A precursor (ZAD, 0.1 M) was mixed with 100 mL of solvent (ethanol), followed by the addition of monoethanolamine (MEA) dropwise to obtain a clear and uniform zincate solution. The zincate solutions were prepared from pure ZnO, 1%, 3% and 5% Al doped content. Film deposition was carried out by dipping the pre-cleaned microscopic glass substrate alternatively in zincate bath, which was kept at room temperature and hot deionized water bath, kept between 90 to 100 ºC. One set of dipping involves 30 s dipping in zincate bath and in a hot deionized water bath. This process was repeated for 30 cycles to obtain the thin film and the film was post annealed at 250 ºC.

Antibacterial activity: *E. coli* (Gram-negative) and *S. aureus* (Gram-positive) bacteria were used for assessing the antibacterial activity of the prepared pure and Al doped ZnO. Agar diffusion method was used for assessing the antibacterial activity. Sterile Muller Hinton (MHA) agar was distributed within sterile petri dishes. The culture specimen was adjusted to 10^8 cfu/mL. The surface of the agar plate was swabbed over using sterile cotton swab. Prepared samples were kept at the middle of the plate and incubated for 24 h at 37 ºC. The incubated plates were then tested for the interruption of growth sample. The diameter of the inhibited growth (ZOI) near the sample was measured.

Antifungal activity: Agar diffusion method was applied for the assay of antifungal activity on ZnO and Al doped ZnO. The antifungal assessment uses potato dextrose agar medium and *Aspergillus niger* was the test organism. A petridish was dispensed with the prepared potato dextrose agar medium and the spores of fungi have been inoculated into sterile distilled water having few glass beads and shaken energetically to take the spores into the suspension. The surface of the agar was diffused uniformly with 1.0 ± 0.1 mL of inoculums. The test samples were set in agar medium and incubated at 27 ºC. The zone of mycosis under and along the sides of the samples was measured after the incubation period. The incubated plates were inspected for interruption in the growth of inoculums. The size of the clear region was noted for assessment of the inhibitory impact of the assessment sample.

RESULTS AND DISCUSSION

Structural analysis: Fig. 1a indicates the X-ray diffraction patterns of pure and aluminium doped ZnO films annealed at 250 ºC. The diffraction peaks observed at (100), (002), (101), (102), (110), (103), (200), (112), (201), (004) and (202) lattice plane confirmed the hexagonal Wurtzite structure of the prepared films as it well matches with the JCPDS card number 36-1451. The film pattern with the highest intensity at the (002) plane reveals the orientation of the particles are along the *c*-axis. This may be owing to the negligible interior stress and surface energy and also because of the high atomic density makes the crystallites grow towards the *c*-axis easily [18,19]. The right shift was observed in the main peak position, which is shown in Fig. 1b. The doped samples illustrate that the planes (100), (002) and (101) exhibits a shift towards the higher angle side. This shift observed in the peak is owing to the attribution of ionic radii of dopant Al^{3+} ion, which is small when compare to Zn^{2+} ion. The peaks also found to broaden with increase in aluminium concentration.

Various structural parameters of pure and Al doped ZnO thin films are shown in Table-1. The crystallite size of the prepared films was calculated using Debye-Scherrer's formula. Table-1 clearly shows that there is a decrease in the crystallite size of Al doped thin film when compared with pure ZnO thin film. It may be because of large number of dislocations and stress created by the ionic radii from Al ions which take up the interstitial sites within the ZnO crystal lattice [20]. Lattice constants for the prepared films are well matched with the standard values. The lattice constant 'a' and 'c' are smaller in Al doped thin films than that of pure ZnO thin film. Incorporation of Al ions into Zn ions leads to compression of lattice because Al^{3+} ion is small than that of Zn^{2+} ion. Obtained crystallite size and the microstrain values indicated that they are sensitive to Al doping. In addition, Fig. 2 shows the changes of the crystallite size along with the microstrain as a function of Al ratio, showing the likely reduction in the crystallite size which may be seen from the diffraction peak broadening as shown in Fig. 1b. The dislocation density of pure ZnO thin

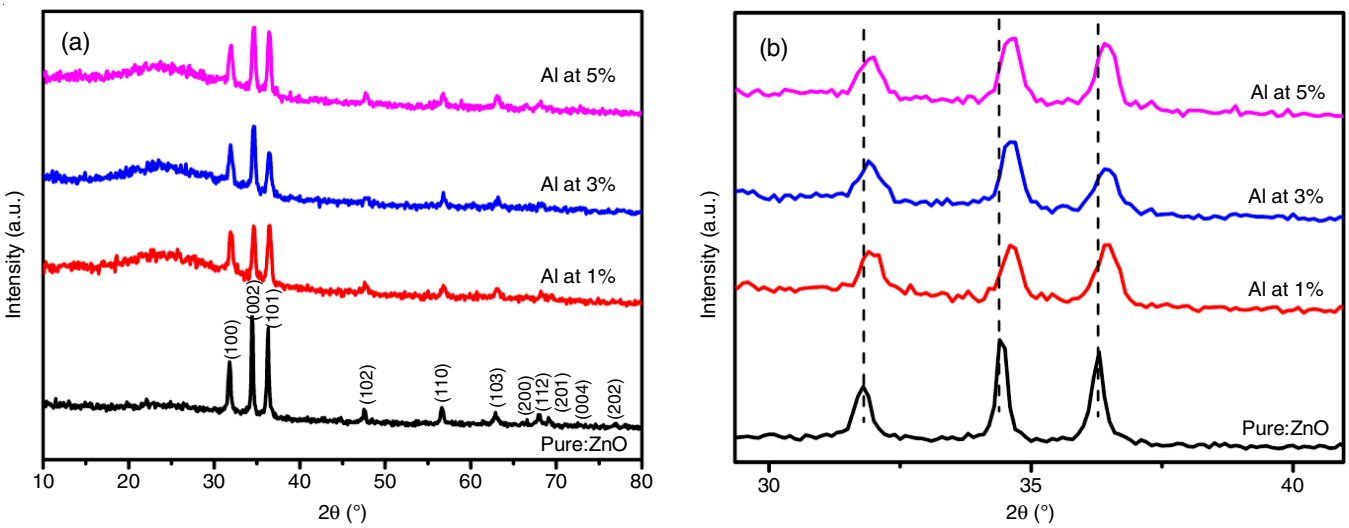

Fig. 1. X-ray diffraction pattern of pure and Al doped ZnO thin films

TABLE-1
STRUCTURAL PARAMETERS OF PURE, 1%, 3% AND 5% Al DOPED ZnO THIN FILMS

Thin film sample	Crystallite size (D) (nm)	Microstrain (ε) × 10^{-3}	Dislocation density (δ) × 10^{15} lines/m^2	Unit cell volume (Å)^3	Lattice constants (Å)	
					A	C
Pure ZnO	30.05	1.2054	1.1085	47.6139	3.2492	5.2075
1% Al	19.27	1.8793	2.6944	47.1123	3.2391	5.1848
3% Al	19.31	1.8756	2.6837	47.0456	3.2381	5.1808
5% Al	18.40	1.9685	2.9562	47.1342	3.2406	5.1825

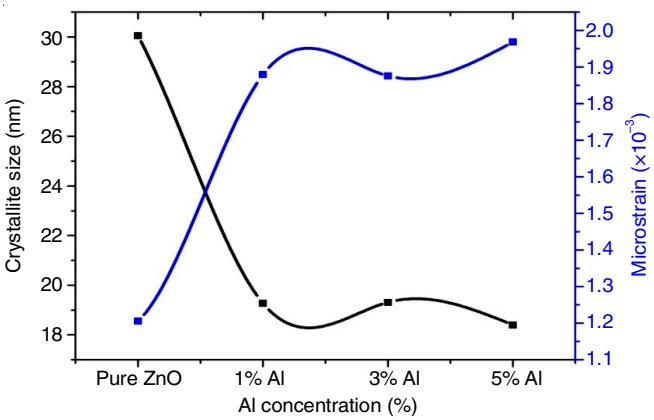

Fig. 2. Aluminium doping effect on crystallite size and microstrain

film was 1.1085 × 10^{15} lines/m^2 and increased to 2.9562 × 10^{15} lines/m^2 after Al doping. These results highlight that there is an increase in lattice imperfection in the Al doped ZnO thin film.

Surface morphology: Fig. 3 illustrates the field emission scanning electron microscope (FESEM) images of Al doped and pure ZnO thin films. Spherical shaped particles are seen in pure ZnO thin film Fig. 3a. FESEM images of Al doped ZnO thin films are shown in Fig. 3b-d. Al doping influences a large change in the grains and modification of spherical shape to hexagonal faced rod like structure. This shape is random in alignment for 1% Al doped ZnO and when the concentration is further increased to 3% and 5%. They exhibit the agglomeration in grains and almost covers the entire substrate surface

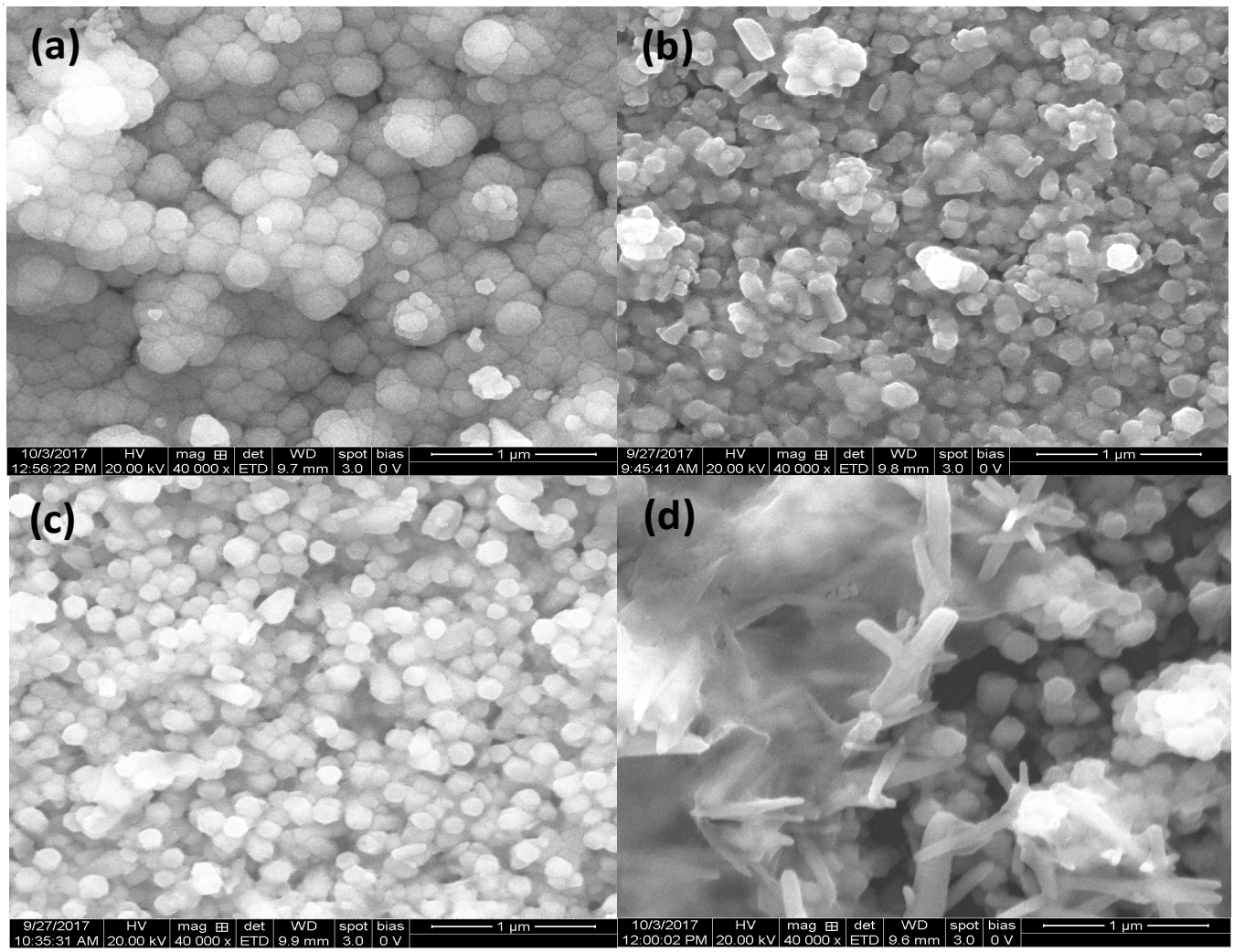

Fig. 3. FESEM images (a) pure, (b) 1% Al, (c) 3% Al and (d) 5% Al doped ZnO thin films

with rod like structure. Such changes in the shape of particles are owed to the formation of quantum properties on the surface and opposite effect of oxide formation of Al-O-Zn [21]. The images clearly indicate that the average crystallite size was decreased with increasing the Al concentration. Hence, it can be presumed that Al doping have a vital part in controlling the morphology of the films.

Fig. 4a-d showed the atomic force microscopy (AFM) morphology of the pure and Al doped (1%, 3% and 5%) ZnO thin films with a scanning area of 3 × 3 micrometer. The surface property for 1%, 3% and 5% Al doped ZnO thin films seems to be thick and are in good quality. A pure ZnO thin film have smooth surface and the surface roughness seems to increase with increase in Al content. The root mean square (RMS) values of films with pure, 1%, 3% and 5% Al concentration were 10.76, 23.87, 34.96 and 44.29, respectively. The average roughness was found to be 5.46, 15.99, 26.30 and 32.98 for pure, 1%, 3% and 5% Al content. The AFM result shows that smoothness of the coating surface decreases with increase in doping concentration [22,23].

EDS analysis: Fig. 5a-d represents the elemental compositions of the prepared samples. It proves the presence of zinc

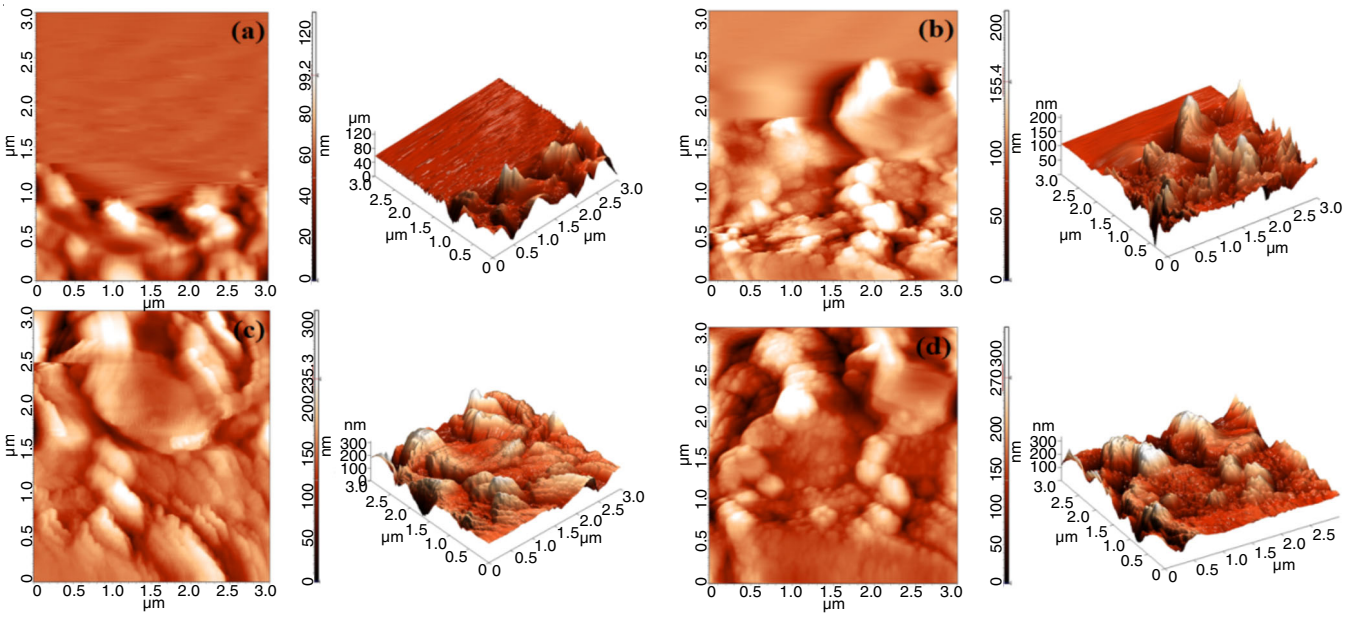

Fig. 4. AFM Images (a) pure, (b) 1% Al, (c) 3% Al and (d) 5% Al doped ZnO thin films

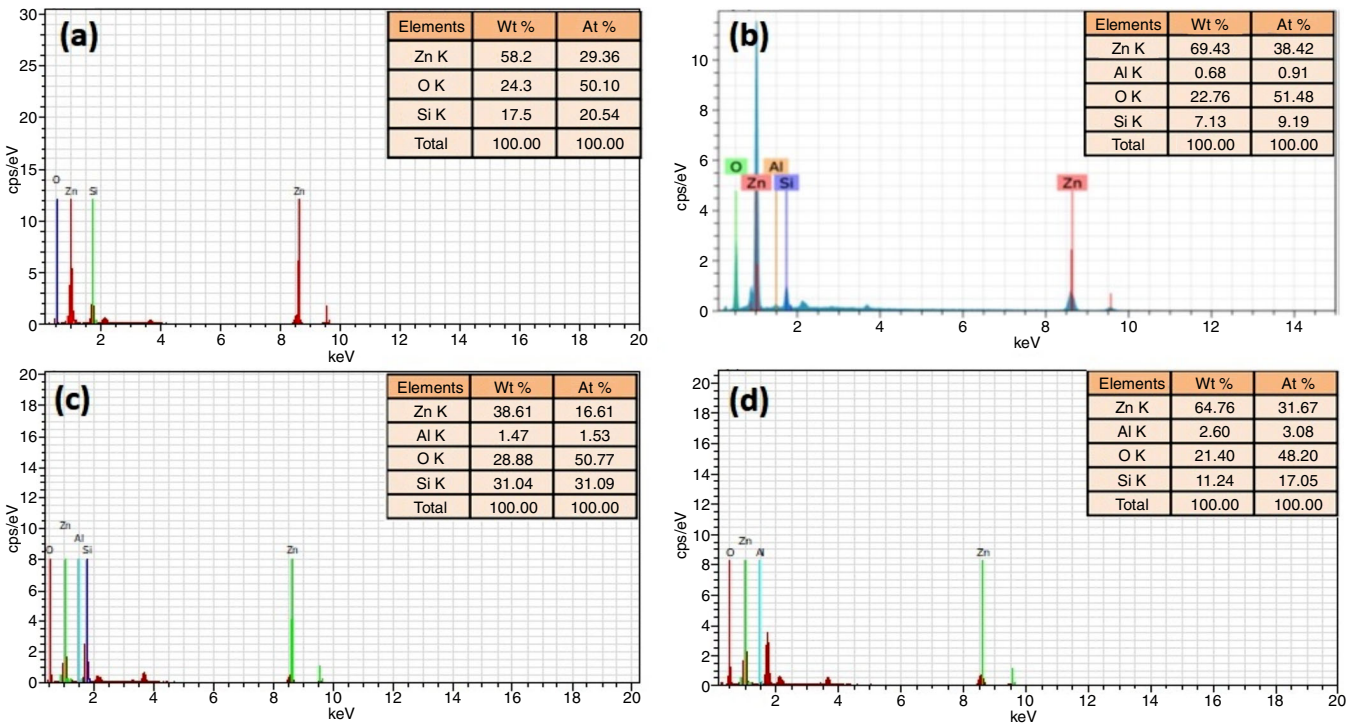

Fig. 5. EDS images (a) pure, (b) 1% Al, (c) 3% Al and (d) 5% Al doped ZnO thin films

and oxygen in pure ZnO thin film and also the incorporation of Al in ZnO thin films. The inset in Fig. 5 gives the ratio of elements present in the film. The silicon peak present in the EDS was originated from the glass substrate. EDS also confirms that Al atomic percent increases from 0.91 to 3.08 with the increase in the doping content.

Optical properties: Fig. 6 illustrates the absorption spectrum of pristine and Al doped ZnO thin films. The absorption spectrum clearly indicates hyperchromic effect with increase in Al doping. Films show a broad absorption in the ultraviolet region from 300-378 nm. The absorption edge was shifted to the lower energy side for Al doped ZnO, such similar results were also seen in Cd doped ZnO thin films [24]. The material has higher optical property in presence of Al and thereby, the absorption band edge increases from 366.67 nm for pure ZnO and to 371.89 nm for 5% Al doped ZnO. The absorption spectra indicate that maximum absorption for 5% Al. This might be due to the doping of Al which affects the density of unsaturated bonds making the deviation of local states within the bandgap.

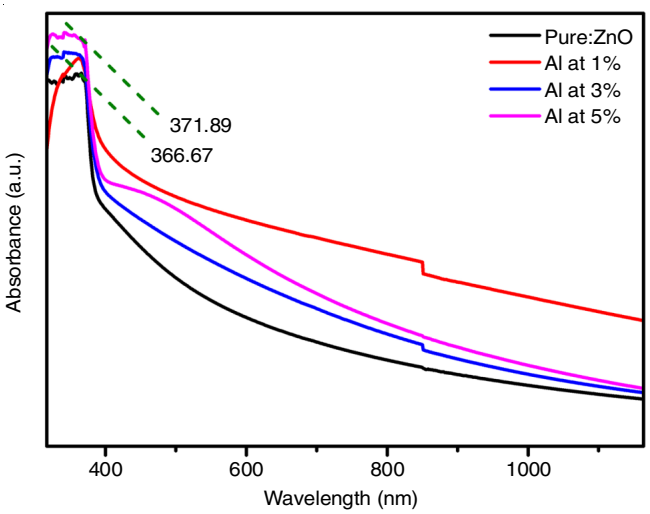

Fig. 6. Absorption spectrum of pure and Al doped ZnO thin films

Fig. 7 represents the relation between $(\alpha h\nu)^2$ and $(h\nu)$ of the prepared ZnO film with different Al contents and the inset denotes bandgap attained by projecting the linear part of the graph and the bandgaps were 3.15, 3.12, 3.10 and 3.06 eV for pure, 1%, 3% and 5% Al doped ZnO thin films, respectively. The bandgap decreases with the doping of Al content and can be explained in terms of stress relaxation mechanism. Such type of red-shift has been reported by Mohanty *et al.* [25]. This suggests the opening of defect states within the bandgap and it can be interpreted due to merging of impurity band into the conduction band, thus shrinking the bandgap.

Photoluminescence studies: The photoluminescence spectra with an excitation wavelength of 325 nm of Al doped ZnO is shown in Fig. 8. It clearly indicates that the films created a narrow ultraviolet (UV) emission peak and a green emission band. The figure clearly shows near band emission at 376-393 nm, which is due to ZnO intrinsic emission produced through the recombination of free excitons [26], while a deep-level

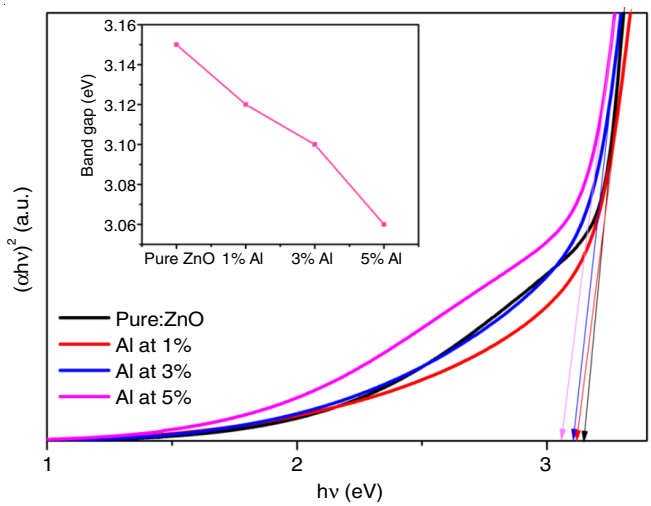

Fig. 7. Plot of $(\alpha h\nu)^2$ *vs.* photon energy $(h\nu)$ of ZnO film with different Al concentration

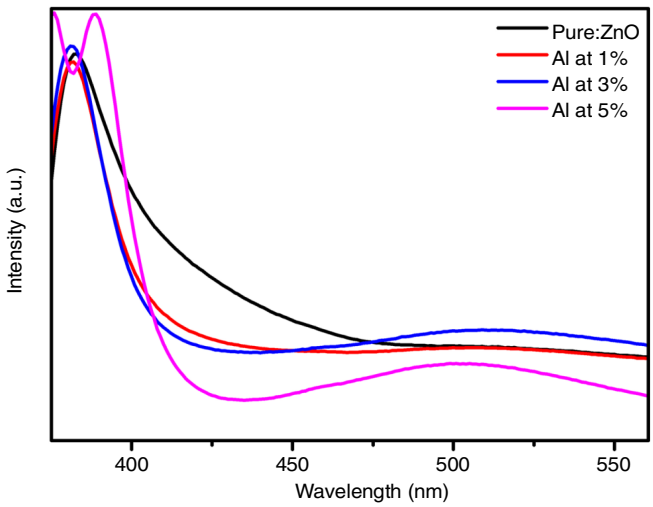

Fig. 8. Photoluminescence spectrum of pure and Al doped ZnO thin films

emission at 450-550 nm is due to the zinc interstitial defects and oxygen vacancies [27].

Antibacterial activity: Aluminium doped ZnO showed significant results as compared to pure ZnO. 5% Al doped ZnO has the maximum zone of inhibition of about 25 mm against *E. coli* and 3% Al doped ZnO has the maximum zone of inhibition of about 21 mm against *S. aureus* (Fig. 9). It is because of the hard bonding of the ZnO elements over the bacteria's external cell membrane. Since then, ZnO particles start to discharge oxygen species into the bacteria which suppress the development of cell which results in the alteration and leakage of the cell and makes the cell to death [28]. The zone of inhibition clearly shows the method of the biocidal activity of aluminium doped ZnO which obliterates the external wall of the bacteria and promotes death [29]. Physico-chemical mechanisms promote different harmful effects on the bacterial cell causing cell wall disarrangement, increase oxidative stress and damaging the nucleic acids which leads to inhibit the growth of the cell and leads to death [30]. The antibacterial effect of Al doped zinc oxide was superior on *E. coli* than other strain. This is because the thickness of the cell wall is thin for Gram-negative bacteria.

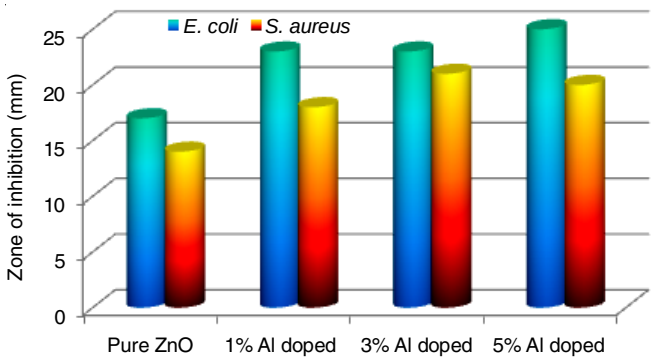

Fig. 9. Antibacterial activity of pure and Al doped ZnO

Antifungal activity against *Aspergillus niger* on pure and Al doped ZnO is shown in Fig. 10. The maximum zone of inhibition after four days of incubation for pure ZnO, 1%, 3% and 5% Al was found to be (18, 10, 10 and 17) mm, respectively. Both doped and pure ZnO shows a significant antifungal activity. The ZnO particles inhibit the development of *Aspergillus niger* by affecting the cellular function, which leads to the deformation in fungal hyphae [31]. The creation of reactive oxygen species (ROS) is responsible for the increase in the permeability of the cell membrane, which enables the cell death.

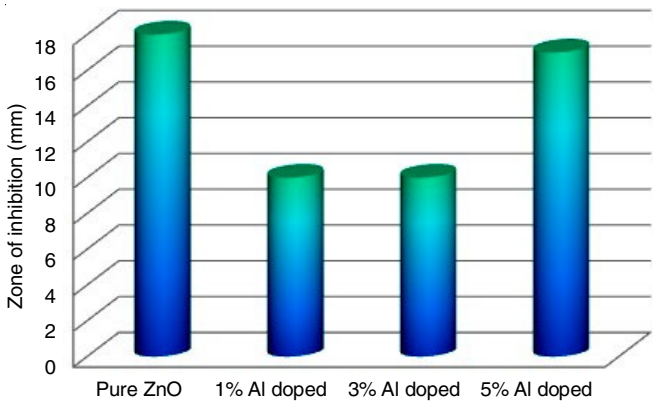

Fig. 10. Antifungal activity of pure and Al doped ZnO

Conclusion

SILAR technique was utilized to prepare pure and Al doped ZnO thin films and the films were post annealed at 250 ºC. The XRD result revealed that every prepared film having hexagonal Wurtzite arrangement and the outcomes are well matched with the standard JCPDS data (card no. 36-1451). Aluminium doping in ZnO influence the crystallite size by decreasing it sharply. FESEM images revealed the spherical morphologies for pure ZnO thin film and hexagonal faced rod like structure for Al doped ZnO thin films. Atomic force microscopic (AFM) study revealed that RMS values increases with the aluminum concentration. In the optical study, a shift towards higher wavelength of the absorption edge was noticed. The bandgap of ZnO was found to decreases with increase in the Al doping concentration. Photoluminescence spectrum shows the existence of near band emission and deep level emission. The antibacterial and antifungal results clearly shows that pure and Al doped ZnO has very good antimicrobial effect on microorganisms.

CONFLICT OF INTEREST

The authors declare that there is no conflict of interests regarding the publication of this article.

REFERENCES

1. O.O. Abegunde, E.T. Akinlabi, O.P. Oladijo, S. Akinlabi and A.U. Ude, *AIMS Mater. Sci.*, **6**, 174 (2019); https://doi.org/10.3934/matersci.2019.2.174
2. F. Dabir, H. Esfahani, F. Bakhtiargonbadi and Z. Khodadadi, *J. Sol-Gel Sci. Technol.*, **96**, 529 (2020); https://doi.org/10.1007/s10971-020-05269-0
3. J. Sawai, E. Kawada, F. Kanou, H. Igarashi, A. Hashimoto, T. Kokugan and M. Shimizu, *J. Chem. Eng. of Jpn*, **29**, 627 (1996); https://doi.org/10.1252/jcej.29.627
4. A.G. Cuevas, K. Balangcod, T. Balangcod and A. Jasmin, *Procedia Eng.*, **68**, 537 (2013); https://doi.org/10.1016/j.proeng.2013.12.218
5. A. Sirelkhatim, S. Mahmud, A. Seeni, N.H.M. Kaus, L.C. Ann, S.K.M. Bakhori, H. Hasan and D. Mohamad, *Nanomicro Lett.*, **7**, 219 (2015); https://doi.org/10.1007/s40820-015-0040-x
6. M.L. Wethimuni, D. Capsoni, M. Malagodi and M. Licchelli, *J. Nanomater.*, **2019**, 6715756 (2019); https://doi.org/10.1155/2019/6715756
7. S.S. Shinde, A.P. Korade, C.H. Bhosale and K.Y. Rajpure, *J. Alloys Compd.*, **551**, 688 (2013); https://doi.org/10.1016/j.jallcom.2012.11.057
8. R. Wahab, A. Mishra, S. Yun, I.H. Hwang, A.A. Al-Khedhairy, Y.-S. Kim, J. Mussarat and H.-S. Shin, *Biomass Bioenergy*, **39**, 227 (2012); https://doi.org/10.1016/j.biombioe.2012.01.005
9. J. Panigrahi, B. Behera, I. Mohanty, U. Subudhi, B.B. Nayak and B.S. Acharya, *Appl. Surf. Sci.*, **258**, 304 (2011); https://doi.org/10.1016/j.apsusc.2011.08.056
10. P. Amornpitoksuk, S. Suwanboon, S. Sangkanu, A. Sukhoom, K. Srijan, J. Wudtipan and S. Kaewtaro, *Powder Technol.*, **212**, 432 (2011); https://doi.org/10.1016/j.powtec.2011.06.028
11. F.K, Mugwang'a, P.K. Karimi, W.K. Njoroge and O. Omayio, *J. Fund. Renew. Energy Appl.*, **5**, 170 (2015).
12. S. Marouf, A. Beniaiche, H. Guessas and A. Azizi, *Mater. Res.*, **20**, 88 (2016); https://doi.org/10.1590/1980-5373-mr-2015-0751
13. M.R. Alfaro Cruz, O. Ceballos-Sanchez, E. Luévano-Hipólito and L.M. Torres-Martínez, *Int. J. Hydrogen Energy*, **43**, 10301 (2018); https://doi.org/10.1016/j.ijhydene.2018.04.054
14. A. Kathalingam, N. Ambika, M.R. Kim, J. Elanchezhiyan, Y.S. Chae and J.K. Rhee, *Mater. Sci. Pol.*, **28**, 513 (2010).
15. N. Lehraki, M.S. Aida, S. Abed, N. Attaf, A. Attaf and M. Poulain, *Curr. Appl. Phys.*, **12**, 1283 (2012); https://doi.org/10.1016/j.cap.2012.03.012
16. G.G. Valle, P. Hammer, S.H. Pulcinelli and C.V. Santilli, *J. Eur. Ceram. Soc.*, **24**, 1009 (2004); https://doi.org/10.1016/S0955-2219(03)00597-1
17. A.C. Nwanya, P.R. Deshmukh, R.U. Osuji, M. Maaza, C.D. Lokhande and F.I. Ezema, *Sens. Actuators B Chem.*, **206**, 671 (2015); https://doi.org/10.1016/j.snb.2014.09.111
18. T. Schuler and M.A. Aegerter, *Thin Solid Films*, **351**, 125 (1999); https://doi.org/10.1016/S0040-6090(99)00211-4
19. S. Bandyopadhyay, G.K. Paul, R. Roy, S.K. Sen and S. Sen, *Mater. Chem. Phys.*, **74**, 83 (2002); https://doi.org/10.1016/S0254-0584(01)00402-3
20. Y. Caglar, M. Caglar and S. Ilican, *Curr. Appl. Phys.*, **12**, 963 (2012); https://doi.org/10.1016/j.cap.2011.12.017
21. R. Mahdavi and S.A. Talesh, *Adv. Powder Technol.*, **28**, 1418 (2017); https://doi.org/10.1016/j.apt.2017.03.014
22. M. Kumar, B. Singh, P. Yadav, V. Bhatt, M. Kumar, A.C. Abhyankar, K. Singh, A. Kumar and J.-H. Yun, *Ceram. Int.*, **43**, 3562 (2017); https://doi.org/10.1016/j.ceramint.2016.11.191

23. D.K. Takci, E.S. Tuzemen, K. Kara, S. Yilmaz, R. Esen and O. Baglayan, *J. Mater. Sci. Mater. Electron.*, **25**, 2078 (2014); https://doi.org/10.1007/s10854-014-1843-0
24. F.K. Shan, G.X. Liu, W.J. Lee and B.C. Shin, *J. Cryst. Growth*, **291**, 328 (2006); https://doi.org/10.1016/j.jcrysgro.2006.03.036
25. B.C. Mohanty, Y.H. Jo, D.H. Yeon, I.J. Choi and Y.S. Cho, *Appl. Phys. Lett.*, **95**, 062103 (2009); https://doi.org/10.1063/1.3202399
26. N.W. Wang, Y.H. Yang and G.W. Yang, *J. Phys. Chem. C*, **113**, 15480 (2009); https://doi.org/10.1021/jp906924w
27. B. Cao, W. Cai and H. Zeng, *Appl. Phys. Lett.*, **88**, 161101 (2006); https://doi.org/10.1063/1.2195694
28. N. Ekthammathat, S. Thongtem, T. Thongtem and A. Phuruangrat, *Powder Technol.*, **254**, 199 (2014); https://doi.org/10.1016/j.powtec.2014.01.010
29. C. Manoharan, G. Pavithra, M. Bououdina, S. Dhanapandian and P. Dhamodharan, *Appl. Nanosci.*, **6**, 815 (2016); https://doi.org/10.1007/s13204-015-0493-8
30. D. Valerini, L. Tammaro, F. Villani, A. Rizzo, I. Caputo, G. Paolella and G. Vigliotta, *J. Mater. Sci.*, **55**, 4830 (2020); https://doi.org/10.1007/s10853-019-04311-z
31. L. He, Y. Liu, A. Mustapha and M. Lin, *Microbiol. Res.*, **166**, 207 (2011); https://doi.org/10.1016/j.micres.2010.03.003